Title

Compression mechanisms of unsaturated clay under high stresses

Journal

Canadian Geotechnical Journal, 52(12)

ISSN

0008-3674

Authors

Mun, Woongju

McCartney, John S

Publication Date

2015-12-01

DOI

10.1139/cgj-2014-0438

Peer reviewed

Compression Mechanisms of Unsaturated Clay under High Stresses

by Woongju Mun, M.S.[1] and John S. McCartney, Ph.D., P.E.[2]

ABSTRACT: This paper investigates the compression behavior of unsaturated clay under mean stresses up to 160 MPa and different drainage conditions. A new isotropic pressure cell was developed that incorporates matric suction control using the axis translation technique, and a high-pressure syringe pump operated in displacement-control mode was used to control the total stress and track specimen volume changes. In addition to presenting results from characterization tests on the cell, results from a series of isotropic compression tests performed on compacted clay specimens under drained and undrained conditions are presented. These results permit evaluation of hardening mechanisms and transition points in the compression curve with increasing effective stress. As expected, specimens tested under undrained conditions were much stiffer than those tested under drained conditions. In the drained tests, the rate of compression was sufficient to permit steady-state dissipation of excess pore water pressure except under the highest stress ranges. Suction-induced hardening was observed when comparing saturated and unsaturated specimens tested in the drained compression tests. In both the drained and undrained compression tests, the range of applied stresses was sufficient to cause collapse or dissolution of the air voids (pressurized saturation) and convergence of the virgin compression lines for unsaturated specimens with that measured for saturated specimens. A gradual transition to full-void closure was observed at high stresses when the compression curves were plotted on a natural scale, but the shapes of the compression curves at high stresses were not consistent with conventional soil mechanics models when plotted on a semi-logarithmic scale. The results from this study provides insight into how constitutive models for unsaturated soils can be extended to high stress conditions for drained and undrained conditions.

KEYWORDS: Unsaturated soil, suction-controlled testing, axis-translation technique, isotropic pressure cell, high stress state

[1] Doctoral Candidate, University of Colorado Boulder, Dept. of Civil, Environmental and Architectural Engineering, UCB 428, Boulder, CO 80309; woongju.mun@colorado.edu

[2] Associate Professor, University of California San Diego, Department of Structural Engineering. 9500 Gilman Dr., La Jolla, CA 92093-0085, mccartney@ucsd.edu.

INTRODUCTION

The rapid release of energy from a shallowly-buried explosive in soil will exert an upward pressure that depends on the compression characteristics of the underlying soil layer. The reaction provided by the underlying soil is influenced by a variety of factors including the depth of burial, soil type, soil density, and soil degree of saturation (Akers 2001). In the case of buried explosives encountered in the field, the near surface soil is typically compacted and partially saturated. Although a buried explosion is a complex, rate-dependent process, many blast simulation models use the parameters of the quasi-static compression curve as important constitutive inputs for the soil behavior (Zimmerman et al. 1987; Akers et al. 1995; Moral et al. 2010). Although compression curves of unsaturated silts and clays have been measured under high mean stresses (greater than 69 MPa) by Hendron et al. (1969) and Mazanti and Holland (1970), the compression behavior of unsaturated soils under constant suction conditions with monitoring of changes in the degree of saturation has only been evaluated under mean stresses up to 10 MPa (Lloret et al. 2003; Jotisankasa 2005; Jotisankasa et al. 2007). Further, there has not been a thorough comparison between the drained and undrained compression curves of unsaturated soils to high stresses. Accordingly, there is a need to characterize transition points in the compression curves of unsaturated soils associated with suction-induced hardening, pressurized saturation (air-void closure), and full-void closure over a wider range of stresses.

The objective of this study is to characterize the isotropic compression behavior of unsaturated, compacted clays under mean stresses as high as 160 MPa. To reach this objective, a high-pressure isotropic pressure cell was developed that permits independent control of the pore air and water pressures within an unsaturated soil specimen along with control of the cell pressure using a syringe pump that permits constant-rate-of-strain compression testing.

Application of mean stresses up to 160 MPa is expected to permit evaluation of the point at which the normally consolidated lines for different suction values converge as the air voids collapse. Although this stress range may not be sufficient to reach full-void closure, which has been observed to occur under stresses as high as 400 to 600 MPa in sands (Akers 2001; Ehrgott et al. 2010), it may be sufficient to detect the onset of the transition to full-void closure.

In addition to presenting a characterization of the cell machine deflections, this paper presents the results from a series of isotropic compression tests on unsaturated, compacted clay specimens performed to understand the roles of initial conditions and drainage conditions, and to highlight transitions in the compression curve over a wide range of stresses. Tests were performed on specimens prepared by compaction at different gravimetric water contents but to the same initial dry density to evaluate the impact of different initial degrees of saturation (and corresponding matric suction values). Although the clay specimens may have anisotropic properties because of the compaction process, the role of anisotropy in the volumetric response may diminish after compression to higher stresses than the preconsolidation stress induced by compaction so it is not explicitly considered in this study. Tests were performed on the specimens under both undrained conditions (no outflow of air or water with varying suction) as well as drained conditions (free outflow of air and water with constant suction). The results were synthesized to evaluate the effects of these variables on the different transition points of the compression curve.

BACKGROUND

In general, the compression of unsaturated soils will occur due to the rearrangement of the soil skeleton, compression of the pore fluids, and compression and potential crushing of the individual particles (Wang & Lu 2003). The deformation of a compacted, unsaturated clay is complex due to the interaction between the different phases. Although the pore air has a much

softer compression response than the pore water, and rearrangement of the soil skeleton may be resisted by capillary pressures (matric suction) related to the air-water surface tension (Matyas & Radakrishna 1968; Wheeler & Sivakumar 1992; Fredlund & Rahardjo 1993). The deformation characteristics of unsaturated soils also depend on the drainage conditions, which are typically considered sensitive to the rate of loading. For example, fast loading is expected to lead to undrained conditions, as the pore fluids may not have sufficient time to drain from the soil pores. The rate of loading required to maintain drained conditions may decrease during compression due to the decrease in void ratio and corresponding hydraulic conductivity, which governs the rate of drainage of pore water from the soil.

It is expected that several key transition points will occur in the compression curves of unsaturated clays over a wide range of mean stresses, as shown schematically in Figure 1. Initial compression of a compacted, unsaturated clay in drained conditions will typically follow a recompression line (RCL) having a slope κ, until reaching the mean apparent preconsolidation stress p_c' that is induced by the compaction process. The particular value of p_c' may depend on the suction magnitude due to the impact of suction-induced hardening (Alonso et al. 1990; Maatouk et al. 1995; Lloret et al. 2003; Jotisankasa 2005; Jotisankasa et al. 2007; Jotisankasa et al. 2009). These studies also observed that the slope of the virgin compression line (λ_s) becomes steeper with increasing suction magnitude when the compression curve is plotted in terms of mean net stress. The impacts of suction on the preconsolidation stress and slope of the virgin compression line (VCL) observed in these studies have been incorporated into most elasto-plastic constitutive models for unsaturated soils (e.g., Alonso et al. 1990). Although some constitutive models assume that the mean net stress and suction have independent effects on the compression behavior of soils, Khalili and Lloret (2001) observed that the use of a single-value

effective stress parameter can be used to unify the compression response of saturated and unsaturated soils. At higher stresses, it is expected that the pore air will be expelled from the soil pores or potentially dissolved into the pore water following Boyle's and Henry's laws (Schuurman 1966). The point at which the air-filled voids are closed is referred to the point of pressurized saturation (air-void closure). When soils are compressed to higher stress under drained conditions, the VCLs for different suction values are expected to collapse to a single VCL at the point of pressurized saturation (Jotisankasa et al. 2007). At very high stresses, it may be possible to reach full-void closure. In sands, full-void closure involves particle crushing and rearrangement that may start occurring at lower stress levels depending on the particle mineralogy (Lee and Seed 1967; Bishop 1966; Vesić and Clough 1968; Murphy 1971; Akers 2001). However, this phenomena has not been observed for clays in previous high-pressure experiments (Hendron et al. 1969; Mazanti and Holland 1970; Murphy 1971; Casey and Germaine 2014).

In a similar manner, initial compression of an unsaturated soil under undrained conditions will also likely follow a recompression curve, potentially with a steeper slope κ_u than that observed in drained conditions. It is uncertain whether suction-induced hardening effects on the value of κ_u or a preconsolidation stress may be observed in undrained compression tests. However, at some point the pore air is expected to be dissolved into the water (Schuurman 1966). At this point, the compression curves for saturated and unsaturated specimens under undrained conditions are expected to converge. Continued deformation beyond the point of air-void closure is only expected due to elastic compression of the water and soil skeleton system (Skempton 1961), although continued particle rearrangement and crushing may still occur.

Some of the transition points in Figure 1 can be observed in a real soil by re-interpreting the compression curves of unsaturated silty clay specimens with different initial degrees of saturation measured in constant water content oedometer tests by Jotisankasa (2005) in terms of mean effective stress, shown in Figure 2(a). The vertical stresses reported by Jotisankasa (2005) were converted to mean stress using a value of $K_0 = 0.46$ estimated from Jaky's equation using the friction angle for this soil of 32.8°. Further, the mean effective stress p´ was calculated using the definition of Bishop (1959), given as follows:

$$p' = p_{net} + \chi\psi \quad (1)$$

where p_{net} is the mean net stress in excess of the pore air pressure, ψ is the suction, and χ is the effective stress parameter which is assumed to equal the degree of saturation ($\chi = S_r$). The change in degree of saturation ΔS_r during compression was calculated from the change in void ratio as the gravimetric water content in the tests by Jotisankasa (2005) was constant ($\Delta S_r = wG_s/\Delta e$, w is the gravimetric water content, G_s is the specific gravity, and e is the void ratio). Accordingly, the degree of saturation curves, also shown in Figure 2(a), are the reverse images of the compression curves. The compression curves for the unsaturated specimens show a greater preconsolidation stress than that for the saturated specimen, although the VCL curves for the unsaturated specimens converge with that of the saturated specimen at a mean effective stress of approximately 1 to 2 MPa depending on the initial degree of saturation. The mean effective stress at which the VCLs converge correspond approximately with the point at which pressurized saturation occurred (i.e., when $S_r = 1$). Although the slopes of the VCLs in Figure 2(a) appear to change at the highest level of stress, this is a phenomena that needs further evaluation. The mean effective stresses at yielding and at pressurized saturation are summarized in Figure 2(b), and indicate that both parameters are higher for specimens with a lower initial degrees of saturation.

After measurement of the compression curve of soils under high stresses, different constitutive relationships can be fitted to the data for use in numerical simulations. The Hybrid-Elastic-Plastic (HEP) constitutive model was developed by Zimmerman et al. (1987) and Akers et al. (1995) to simulate the behavior of geologic materials during blast loading. The HEP model uses a similar segmental log-linear pressure-compression relationship to that presented in Figure 1 for soils under drained loading. The model was developed for granular materials, so one of the key transition points in the curve that is not shown in Figure 1 is the mean stress at which particle crushing commences, which may not be observed in clays. Nonetheless, the segmental nature of the pressure-compression relationship in the model indicates that additional transition points for the suction-dependent preconsolidation stress and pressure saturation can be readily incorporated. The model also requires measurement of an intermediate unloading curve and a final unloading curve after reaching void closure. The HEP model has been implemented in several numerical codes that describe the blast-induced behavior of soils, including SABER-1D (Zimmerman et al. 1992) and EPIC (Johnson et al. 2006).

MATERIAL

A low plasticity clay obtained from a soil stockpile at a construction site on the University of Colorado Boulder campus was selected a test material for this study, and is referred to as Boulder clay. The clay was air-dried, crushed, and processed after collection to remove all particles greater than the #10 sieve (aperture of 2 mm), which provided a more homogeneous and consistent material for experimental testing. Soil classification tests were performed on Boulder clay to measure the relevant geotechnical properties. The relevant geotechnical properties of the clay are summarized in Table 1. Boulder clay is classified as low plasticity clay (CL) according to the Unified Soil Classification System (USCS). Results from a standard Proctor compaction

test shown in Figure 3(a) indicate that the optimal water content is 17.5% and the maximum dry unit weight is 17.4 kN/m^3. The tests performed on Boulder clay in this study involved specimens compacted to a dry unit weight of 17.5 kN/m^3, which corresponds to an initial void ratio of 0.51, but prepared at different initial gravimetric water contents to evaluate the role of the initial degree of saturation. The Transient Water Release and Imbibition Method (TRIM) of Wayllace & Lu (2012) was used to infer the drying and wetting paths of the soil water retention curve (SWRC) for a Boulder clay specimen having the same initial void ratio as that used in the compression tests (0.51), as shown in Figure 3(b). The parameters of the van Genuchten (1980) SWRC model (α, n, θ_s, θ_r) for the soil are also shown in the figure. Further, the initial suction-saturation points for the specimens tested in this study are also shown in the figure, which both fall on the drying path curve of the SWRC.

EXPERIMENTAL SETUP

A picture and sketch of the components of the experimental setup are shown in Figures 4(a) and 4(b), respectively. The setup incorporates an isotropic pressure cell used to contain the soil specimen, a high-pressure syringe pump (model 65HP from Teledyne Isco) used to apply the cell pressure and track changes in volume of the soil specimen, and a pressure control panel used to control the pore air and water pressures. When provided a target cell pressure, the system controller in the pump will direct a piston into or out of the pump reservoir until the target pressure is met in accordance with a set of input variables defining the tolerance of the system. Details of the syringe pump are summarized in Table 2. Pressures are delivered from the syringe pump to the test cell using hydraulic oil through steel tubing which has the strength of 240 MPa. Automotive brake fluid was selected for the cell fluid due to its high bulk modulus (2.068 GPa) and because it is easy to remove from the equipment after testing.

The pressure cell consists of a hollow stainless steel cylinder sandwiched between two 50.8 mm-thick plate. A 38.1 mm-thick, 71.1 mm-diameter bottom platen used for mounting of the specimen is integrated into the bottom plate. A schematic view of the pressure cell is shown in Figure 5(a), and a picture of the assembled cell is shown in Figure 5(a). A stainless steel load frame with 76.2 mm-thick plates held together with six steel alloy rods is used to resist the pressure within the cell. Before pressurizing the cell, the rods of the load frame are pre-stressed to a torque of 2,983 N·m. The inside of the top plate is slightly tapered toward a flush valve so that air can be evacuated from the cell as it is filled with hydraulic fluid. The cell has five ports in the bottom plate. Two ports are used to supply and flush water to the bottom platen, two port are used to supply and flush air to the bottom platen, and one port is used to supply the hydraulic fluid to the cell. Dual rubber membranes, each with a thickness of 0.64 mm, are used to confine the soil specimen.

A schematic view and photos of the bottom platen of the cell are shown in Figure 6. The pore air pressure in the specimen is applied via a porous sintered stainless ring in the bottom platen of the pressure cell. The pore water pressure in the specimen is applied via a ceramic disk also in the bottom platen of the pressure cell having a high air-entry (HAE) suction which only permits water to pass until reaching a suction of 300 kPa. The recess in the bottom platen that houses the HAE ceramic disk includes a grooved flushing path that allows for uniform distribution of water pressure underneath the disk. Water was supplied from and drained to the exterior via 1 holes located at both ends of the grooved channel. Air was also supplied from the exterior via 1.59 mm-diameter holes located at both ends of the circular grooved channel underneath the sintered ring.

Pore air pressure (u_a) and pore water pressure (u_w) are applied to the specimen through two independent burettes that are included in a pressure control panel. Each burette allows for the unique application of air/water pressure, vacuum pressure, or venting. In addition, each burette is controlled and monitored calibrated pressure gauge. During compression, the change of degree of saturation of the soil specimen is monitored by tracking the outflow or inflow of water from the specimen using a differential pressure transducer (DPT) connected to the pore water pressure burette. As the compressibility of air is relatively high, dissolved air inside the water could negatively impact the accuracy of mechanical response for high pressure testing, so it is important to ensure that all water is de-aired prior to testing. The pressure control panel also includes a third burette to apply a seating cell pressure at the beginning of testing, which facilitates the flushing of air from the system. The cell pressure burette is also used to flush air from the high-pressure syringe pump and can be controlled by an independent pressure gauge to permit the application of the net stress easily before compression testing. When the syringe pump is activated, the supply line from cell pressure control burette is closed using a high pressure valve so that operation of the pump leads to inflow or outflow from the cell.

A saturation cap was constructed to initially saturate the HAE ceramic disk before testing. After placement of the saturation cap over the bottom platen as shown in Figure 7, the entire system was placed under a vacuum of -75 kPa to fully de-air the system. Next, de-aired water was passed through the flushing paths above and below the HAE ceramic. While maintaining the water beneath the porous stone at a vacuum of -75 kPa, water was permitted to flush downward through the HAE disk for several hours. Because of this saturation procedure and because the axis translation tests on soils reported later in this study were all performed under backpressure,

cavitation or dissolution of air were not observed in the water flowing from the base of the HAE ceramic disk.

SYSTEM CALIBRATION

Before testing of the soil specimens, the machine deflections of experimental setup was evaluated using an aluminum specimen with known elastic properties (Young's modulus of 69 GPa and Poisson's ratio of 0.334). The aluminum specimen with a diameter and height of 71.1 mm was first placed into the pressure cell and covered with the membrane. The cell was then filled with hydraulic fluid and pressurized. Using the high-pressure syringe pump, the aluminum specimen was subjected to an isotropic loading and unloading cycle from 0 to 160 MPa and back under a volumetric strain of 2 %/min. The rate of the syringe pump is controlled to ensure that the level of over-estimated pressure is marginalized. Pressure and total volume change provided by the high-pressure syringe pump including refilling process and pressure and cumulative total volume change with operation time are shown in Figures 8(a) and 8(b), respectively. The slight initial non-linear shape reflects the pre-stress of the bolts of the loading frame. It is important to maintain the pressure inside the chamber when testing materials under high pressures so that the precise pressure-deformation relationship can be obtained. In order to verify that the cell held pressure with minimal creep relaxation, the operation of the syringe pump was stopped for some time. The results show that constant pressure was maintained for an hour while the pump was stopped. The pressure effect can be observed from the subtraction of the measured data with the displacement of the aluminum specimen, shown in Figure 9. The equation fitted to the experimental machine deflection data is shown in this figure, which facilitated application of the machine deflection of the cell to interpret deformation results of soil specimens.

EXPERIMENTAL PROCEDURES

A series of suction-controlled isotropic compression tests under mean stresses up to 160 MPa were performed. This stress range is suitable for evaluation of the point at which the normally consolidated lines for different suction values converge as the air voids are compressed (air-void closure), and potentially the point of full-void closure. Both specimen deformation and changes in the volume of water flowing in and out of the specimen were monitored while performing tests. The compression behavior of the unsaturated soil specimens under undrained conditions was also investigated over the same stress range in order to consider the impact of drainage conditions.

Several tests were performed with different initial suctions and drainage conditions. Compacted specimens of Boulder clay were prepared in two lifts using static compaction with a mechanical press to an initial void ratio of approximately 0.51. The compacted cylindrical soil specimens have a diameter and height of 71.1 mm (1:1 ratio). Different target initial degrees of saturation of 1.00, 0.90, and 0.80 were chosen with the same target dry unit weight of 17.5 kN/m^3, respectively. The specimens with S_r of 1.00 were prepared at the same compaction water content as the specimens with S_r of 0.90, but were then saturated by upward imbibition as will be discussed in the next paragraph. The target dry unit weight and gravimetric water content of the specimens at the beginning of compression are listed in Table 3.

To perform compression tests on saturated specimens of Boulder clay, the compacted specimens were first placed within a membrane in the cell, and the saturation cap used to saturate the HAE disk was placed on top of the specimen. Next, a vacuum of -75 kPa was applied to the top of the specimen for at least 1 hour. Next, de-aired water was permitted to flush upwards through the specimen while vacuum was maintained on the top. After flushing several pore

275 volumes of water through the specimen, the saturation cap was then carefully replaced with the
276 rigid top cap (that does not have drainage ports). Then the cell pressure and (water) backpressure
277 were applied to the specimen in stages until a value of Skempton's B parameter remained
278 constant with additional increases in backpressure. In this study, a cell pressure of 483 kPa and a
279 backpressure of 448 kPa were applied and B parameters greater than 0.95 were measured.

280 The tests on unsaturated Boulder clay specimens were performed at their initial suction values
281 resulting from the compaction process. In order to perform drained tests at these initial suction
282 values, a UMS T5 tensiometer was first used to measure the initial values of suction within the
283 specimen as shown in Figure 10. Then the measured suction values were applied to the
284 specimens using the axis translation technique to permit drained compression testing. In this case,
285 positive air and water pressures are applied independently to the base of the specimen, with a
286 difference $u_a - u_w$ being equal to the matric suction in the specimen. Because the same suction
287 that was measured in the specimen was subsequently applied using the axis translation technique,
288 no flow of water or air was expected from the specimen during this process. In the case of soil
289 specimens with higher degrees of saturation such as those evaluated in this study, it is possible
290 that the air pressure applied at the boundary of the specimen may be different from that in
291 occluded air bubbles within the specimen. However, the axis translation approach followed in
292 this study permits application of a constant suction boundary condition to the specimen.
293 Although the suction value could have been be modified in the specimen from the initial value
294 using the axis translation approach, this approach was not employed in this study. Specifically,
295 the top cap used in the compression tests does not include plumbing connections due to concerns
296 that the high cell pressure would compress the tubing, which means that water flow or air could
297 not be facilitated across the height of the specimen. Nonetheless, performing tests on unsaturated

soil specimens at their initial compacted condition still permits new insight into to the compression behavior of these materials under high stresses.

After establishing the initial stress state in the saturated and unsaturated specimens, mean stresses were applied isotropically to the specimens at a constant rate using the syringe pump, up to a cell pressure of 160 MPa. For the drained compression tests, the rate was selected to maintain steady-state drainage during compression. Although the ASTM standard for constant rate of strain testing (ASTM4186/4186M) provides guidance on selecting a practical loading rate in terms of testing time it does not consider the impact of the lower hydraulic conductivity of the unsaturated clay or the change in hydraulic conductivity with void ratio at high stresses. A preliminary series of compression tests were performed on Boulder clay to identify the right balance between drainage and testing time, and a constant volumetric strain rate of 1 %/hr was found to provide a good balance. An evaluation of the adequacy of this rate in providing drainage will be presented in the analysis section. For the undrained compression tests, the loading rate was assumed to not have as great of an effect on the compression response. However, a relatively slow rate of 2 %/hr was still used for the undrained compression tests because the process of pressurized-saturation is likely time dependent (Schuurman 1966).

RESULTS

Undrained Compression Tests

A series of undrained isotropic compression tests under mean stresses up to 160 MPa are conducted for clay specimen with several initial degrees of saturation (S_r=1.0, 0.9, 0.8). The plot of applied mean stresses versus measured volume change for the saturated soil specimen is shown in Figure 11(a). The actual deformations of the soil were defined by subtracting the machine deflections from the measured volume change from the pump during the test. The

relationships between mean stress and volume change for the soil specimens were compared with that of water having a bulk modulus of 2.2 GPa (at atmospheric pressure and room temperature of 20 °C) in order to assess the validity of the test results, as shown in Figure 11(b). The results indicate that the stress response curves for unsaturated Boulder clay have a bend in the curve that likely corresponds to the point at which pressurized saturation occurs. For mean stresses greater than bends in the curves, the compression of the soil is primarily controlled by the pore water. However, the fact that the saturated specimen shows a slightly softer response than that of water indicates that the soil skeleton may also have a slight effect on the undrained compression response.

The undrained compression curves of the compacted specimens with various initial degrees of saturation are shown in Figure 12. These curves show a downward shift with decreasing initial degree of saturation, which corresponds to the lower initial bulk moduli of the drier soil specimens. Although pressurized saturation occurred during undrained compression for all three specimens, the softer initial response for the unsaturated specimens is controlled by the presence of air-filled voids.

Drained Compression Tests

The drained tests for the saturated and unsaturated Boulder clay specimens under constant suction were performed for isotropic stresses up to 160 MPa. During application of the initial suction to the unsaturated specimens using the axis translation technique, the mean stress, pore air pressure, and pore water pressure were increased in stages, as shown in Figure 13. During this process, the initial net stress is constant and equal to 35 kPa, and the initial suction is also constant. Next, isotropic stresses were applied to the specimen up to 160 MPa under drained conditions with volumetric strain rates of 1.0 %/hr.

344 The different amounts of outflow water for the specimens with initial degrees of saturation of
345 1.0, 0.9, and 0.8 are shown in Figures 14(a), 14(b) and 14(c), respectively. The results show that
346 the amount of outflow increases as the initial degree of saturation increases. As observed in
347 Figures 14(b) and 14(c), water started to flow out of the unsaturated specimens after a certain
348 level of stress was reached, whereas the water in the saturated specimen started to flow out
349 immediately after stress application. If a specimen is compressed under drained conditions, water
350 should flow out of the specimen at a constant rate (Gibson & Henkel 1954). Further, water
351 should be drawn back into the specimen when it is unloaded. The results in these figures indicate
352 that the rates of loading used in the tests may not have been slow enough for the unsaturated clay
353 specimens, as water was not drawn back into the specimen completely during unloading.

354 The difference between the total volume change and the outflow of water for specimens with
355 different initial degrees of saturation is shown in Figure 15. The volume change behavior of the
356 soil specimen should be similar to the total volume and void volume after air in the void of soil
357 was totally compressed. This result is attributed to the void of specimen filled with water. As for
358 saturated soil, the results indicate that the volume of water outflow is consistent with the volume
359 change of the soil until the specimen becomes very dense, as shown in Figure 15(a). The
360 difference between the water outflow and the void of soil specimen increases as the initial degree
361 of saturation becomes higher. The behavior of the water outflow becomes similar to the change
362 in soil volume after reaching a mean stress of approximately 4 MPa, as shown in Figures 15(b)
363 and 15(c). In other words, the compression curves for specimens with lower initial degrees of
364 saturation indicate that unsaturated soils behave like saturated soil after reaching the point of
365 pressurized saturation.

As a result, a 1:1 trend between ΔV_w and ΔV_v can be expected for the saturated and unsaturated soil specimens, especially after the point of pressurized saturation. The change of void volume as a function of water outflow is shown in order to identify the effect of initial degree of saturation as seen in Figure 16. The result for the saturated specimen shows that the slope is almost equal to even though the amount of water drainage decreases at high stress (approximately after 20,000 kPa). The compression curves for the unsaturated soil specimens show a significant change in volume at the beginning of stress application, after which the trend approaches a 1:1 slope. This corresponds to mean stresses of 3,600 and 4,300 kPa, respectively, for the specimens with initial degrees of saturation of 0.9 and 0.8. The results for unsaturated specimens indicate that the amount of change in the volume of voids increases as the initial degree of saturation falls due to the compression of air before the start of pressurized saturation.

Since the void ratios are monitored during the compression through the measurement of the volumetric strains and outflow of water from the soil specimen, the change in the degree of saturation can also be estimated based on the known water content for the unsaturated specimens. The change in the degree of saturation with mean effective stress for specimens with different initial degrees of saturation is shown in Figure 17. The result shows that the point where S_r reaches 1.0 for the specimen initially at $S_r = 0.9$ occurred at a relatively low level of stress due to the high initial degree of saturation. Air in the voids may have compressed at a very low stress level around 700 kPa and the change in S_r cannot be seen in the graph after the pressurized saturation. This is because there was no chance for water to be drawn back into the specimen during the unloading process due to the effects of excess pore water pressures, which did not have time to dissipate. On the other hand, the mean stress at the point of pressurized saturation appears to be higher for the test on the specimen initially at $S_r = 0.8$ (around 1,800 kPa).

389 The drained compression curves for Boulder clay specimens having different initial degrees
390 of saturation are shown in Figure 18(a) in terms of void ratio against the logarithm of mean
391 effective stress. The detailed results from the drained tests are listed in Table 4. The mean
392 effective preconsolidation stress is influenced by the degree of saturation, increasing from
393 110 kPa for the specimen with an initial S_r of 1.0 to 580 kPa for the specimen with an initial S_r of
394 0.8. Then, the VCLs with various initial degrees of saturation converge toward the saturated soil
395 VCL at a mean effective stress of approximately 1500 kPa and the effect of initial degree of
396 saturation becomes less prominent. This result confirms the hypothesis on the pressurized
397 saturation after which the effect of suction is marginalized. During the unloading-reloading cycle,
398 all three Boulder clay specimens show similar behavior, although the unsaturated specimens
399 show slightly greater slopes of the RCL. The unloading rate may have been too fast in these tests
400 to permit water to fully retract into the specimens in a drained manner.

401 To better investigate the role of suction induced hardening, the void ratio of the soil
402 specimens is plotted a function of mean effective stress on a natural scale in Figure 18(b) up until
403 the point of pressurized saturation. The effect of the initial degree of saturation and the suction
404 hardening effect is clearly observed in the figure. Specifically, the rate of change in the void ratio
405 is higher for the specimen with an initial S_r of 1.0 compared to those for the specimens with an
406 initial S_r of 0.9 or 0.8 when the applied stresses are relatively low. However, at stresses between
407 1000 and 2000 kPa, all three compression curves converge on a single line with an initial S_r of
408 1.0. It should also be noted that the incipient stage of compression behavior with an initial S_r of
409 0.8 seems to be contrary to that of 1.0 in terms of the changes in slope of the curve, due to the
410 initial impact of suction on the specimen. In other words, while the compression behavior of the
411 specimen having an initial S_r of 1.0 follows an L-shaped curve, the specimen having an initial S_r

412 of 0.8 is displayed in S-shaped curve. Although such a difference is subtle in a natural scale, it
413 appears to be magnified when expressed in a logarithmic scale.

414 An interesting observation from Figure 18(a) is that for mean effective stresses greater than
415 about 30 MPa, it appears that the slopes of the VCLs become steeper than at the beginning of the
416 compression (suction-induced hardening). Although this feature is partially due to the semi-
417 logarithmic scale, it is not consistent with conventional soil mechanics theories that assume a
418 log-linear VCL over the full range of stresses. This may potentially due to the transition toward
419 full-void closure. To better investigate this behavior, the void ratio of the soil specimens is
420 plotted a function of mean effective stress on a natural scale in Figure 18(c) for the full range of
421 stress. The shapes of the compression curves indicate an asymptotic trend toward a certain void
422 ratio, in a similar manner to the natural-scale compression curves for low plasticity clays
423 measured by Hendron et al. (1969) and Mazanti and Holland (1971) and those for sand measured
424 by Murphy et al. (1971). This may reflect that the Boulder clay is transitioning toward full-void
425 closure at stresses greater than about 30 MPa. Another interesting observation from the
426 compression curves in Figures 18(a) and 18(b) is that the curves for the specimens with lower
427 initial degrees of saturation show slightly less volume change at high stresses, even though they
428 are all saturated. This observation may be due to the initial soil structure induced by compaction
429 of the unsaturated specimens to different water contents. Although the specimens with initial
430 degrees of saturation of 1.0 and 0.9 have similar compaction conditions, the specimen with an
431 initial degree of saturation of 0.8 was compacted dry of optimum and may have an initially
432 flocculated soil structure that has an effect on the behavior under high stresses.

433 As mentioned, the compression behavior of the soil specimens under high stresses may not be
434 fully representative of drained conditions due to the decrease in hydraulic conductivity of the soil

as it was compressed. Accordingly, at high stresses these tests do not satisfy the assumption from ASTM D4186 that the coefficient of volume compressibility or hydraulic conductivity are constant. Nonetheless, if the tests were performed at a slower rate such that full drainage would have occurred, it is expected that slightly greater decreases in void ratio would occur for stresses greater than 30 MPa, exacerbating the increase in the slope of the VCLs observed in Figure 18(a). The transition toward full-void closure possibly occurs due to the deformation of the clay particles to fill the voids, or due to the drainage of hydroscopically-bound water. Although it is possible that particle crushing could have occurred, this was not evaluated as it would have required high intensity microscopic imaging. Particle crushing in clays under high stresses is a subject that requires further research.

ANALYSIS

Assessment of the Impact of Initial Conditions

Alonso et al. (1990) developed the concept of the loading-collapse (LC) curve to show the relationship between the mean preconsolidation stress (obtained from a plot of the void ratio versus mean net stress) and the suction. The LC curve is a useful tool to quantify the suction induced hardening behavior for a given soil. The mathematical expression for the LC curve proposed by Alonso et al. (1990) is given as follows:

$$\left(\frac{p_0}{p^c}\right)=\left(\frac{p_0^*}{p^c}\right)^{[\lambda(0)-\kappa]/[\lambda(\psi)-\kappa]} \tag{2}$$

Where p^c is a reference stress state at which one may reach the saturated virgin state starting from unsaturated conditions, and p_0* is the preconsolidation stress for saturated soil. This expression defines the set of the preconsolidation stress values (p_0) for each associated suction (ψ). The value of $\lambda(\psi)$ represents the stiffness parameter that can be expressed as follows:

$$\lambda(\psi) = \lambda(0)\left[(1-r)e^{(-\beta\psi)} + r\right]\lambda(\psi) = \lambda(0)[(1-r)\,exp(-\beta\psi) + r] \quad (3)$$

where λ(0) is the preconsolidation stress at zero suction, r is a constant related to the maximum stiffness of the soil for an infinite suction, and β is a parameter which controls the rate of increase of preconsolidation stress (and associated stiffness) with suction.

The mean preconsolidation stress values inferred from the drained compression curves (in terms of mean net stress) for Boulder clay along with those for silty clay measured by Jotisankasa et al. (2009) are shown in Figure 19(a). The fitting parameters for the LC curves in Figure 19(a) are listed in Table 5. The results indicate that an increase in the preconsolidation stress occurs with increasing suction magnitude. The mean preconsolidation stresses observed for Boulder clay are higher than those of the silty clay tested by Jotisankasa et al. (2009), which may be attributed to the soil mineralogy and higher initial density. The slopes of the VCL and RCL for specimens of Boulder clay with various initial degrees of saturation and different drainage conditions are shown in Figure 19(b). The results indicate that the slope of the drained compression line (λ_s) becomes steeper with decreasing initial degree of saturation. The slope of RCL of the unsaturated specimens in drained conditions (κ) is similar to the slope of the undrained compression line (κ_u), although the values started to deviate with decreasing initial degrees of saturation.

Assessment of the Impact of Drainage Conditions

A comparison between the compression curves for Boulder clay specimens having different drainage conditions and initial degrees of saturation is shown in Figure 20(a). The drained curves are shown in terms of mean net stress while the undrained compression curves are shown in terms of the mean total stress for ease of comparison as it was not possible to estimate the mean

effective stress in the undrained compression tests. As expected, the results show that compacted clay under undrained compression was much stiffer than in drained compression. For the undrained compression, deformations occur due to the compression of the air-filled voids until reaching the point of pressurized saturation (air-void closure). The bulk moduli of the undrained specimens increases at stresses above the pressurized saturation, as specimen compressibility is controlled by the less compressible pore water and particles. Comparing the drained compression curves with that of the compression curve for the saturated specimen under undrained conditions, the shapes of the curves are similar for stresses greater than 30 MPa. This may be due to the decrease in hydraulic conductivity of the specimens compressed in drained conditions. Specifically, the lower hydraulic conductivity may lead to relatively undrained conditions within the specimen even though drainage is provided at the boundaries. If the rate of compression was slower to permit full drainage at the higher range of stresses, a greater decrease in void ratio for the same applied stresses would have been observed. The change of outflow rate can be used as a proxy to examine the soil behavior under high stresses since it is related to the dissipation of excess pore water pressures generated from the application of stresses at a constant rate. A comparison between the rate of outflow and the stress application during compression for a saturated specimen of Boulder clay is shown in Figure 20(b). The outflow rate is observed to decrease asymptotically as the mean effective stress is increased. However, a sharp decrease reflecting a significant decrease in hydraulic conductivity is not observed. This would have been expected if full void closure had occurred.

A comparison of the effect of drainage conditions on the pressurized saturation (air-void closure) in Boulder clay and in the silty clay tested by Jotisankasa (2005) is shown in Figure 21. The result indicates that the mean stress at pressurized saturation for the specimens tested under

undrained conditions is higher than that for specimens tested under drained conditions, which makes sense as air can escape from the specimens tested under drained conditions. Pressurized saturation occurred at a lower mean stress for the silty clay evaluated in a constant water content test by Jotisankasa (2005). Although the cause of the difference could be the soil properties, the tests on the two soils were also conducted under different drainage conditions and stress paths. In case of the drained tests performed on Boulder clay, the suction is forced to be constant, while in the case of the constant water content test, the suction is permitted to change.

CONCLUSION

The compression behavior of compacted clay specimens with various initial degrees of saturation and different drainage conditions was evaluated using a newly developed isotropic pressure cell under mean stresses up to 160 MPa. Overall, the compression curves for compacted soils under drained and undrained conditions confirm the presence of hypothetical transition points for different compression mechanisms of unsaturated soil under high stresses. The initial degrees of saturation was found to play an important role in values of the mean preconsolidation stress, the point of pressurized saturation (air-void closure) interpreted from the compression curves. At high pressures, the compression curves for specimens with different initial degrees of saturation tended to converge with the curve for saturated conditions. As the compression curves at high stresses follow different trends than expected from conventional soil mechanics theories, potentially due to the transition to full-void closure. These observations indicate that caution should be used when extrapolating the slope of the VCL from low to high stresses. Although further research on different soil types is necessary to extend constitutive relationships for the compression of unsaturated soils to high stresses, the transition points observed in the compression curves in this study provide insight into how these relationships can be defined.

ACKNOWLEDGEMENTS

Funding for this research was provided by Office of Naval Research (ONR) grant N00014-11-1-0691. Special thanks are given to Alexandra Wayllace, Yi Dong, and Ning Lu at Colorado School of Mines for measuring the soil-water retention curve for Boulder clay. The opinions in this paper are those of the authors alone.

REFERENCES

Akers, S.A. 2001. Two-Dimensional Finite Element Analysis of Porous Geomaterials at Multikilobar Stress Levels. Ph.D. Thesis, Department of Civil Engineering, Virginia Tech, Blacksburg, VA.

Akers, S.A., Reed, P.A., & Ehrgott, J.Q. 1986. WES high-pressure uniaxial strain and triaxial shear test equipment. Miscellaneous Paper SL-86-11. US Army Engineer Waterways Experiment Station. Vicksburg, MS.

Akers, S.A., Adley, M.D., & Cargile, J.D. 1995. Comparison of constitutive models for geologic materials used in penetration and ground shock calculations. Proceedings of the 7th International Symposium on Interaction of the Effects of Munitions with Structures, Mannheim, Germany.

Alonso, E.E., Gens, A., & Josa, A. 1990. "A constitutive model for partly saturated soils." Géotechnique, 40(3), 405-430.

ASTM D4186/4186M. Standard Test Method for One-Dimensional Consolidation Properties of Saturated Cohesive Soils Using Controlled-Strain Loading. ASTM International, West Conshohocken, PA.

544 Bishop, A.W. 1959. "The principle of effective stress." Teknisk Ukeblad I Samarbeide Med
545 Teknikk, Oslo, Norway. 106(39), 859-863.

546 Bishop, A.W. 1966. "The strength of soils as engineering materials." Géotechnique. 16: 89-130.

547 Casey, B. & Germaine, J.T. (2014). "An evaluation of three triaxial systems with results from 0.1
548 to 100MPa." Geotechnical Testing Journal. 37(6), 1-7. DOI:10.1520/GTJ20130178.

549 Delage, P., Romero, E., & Tarantino, A. 2008. "Recent developments of controlling and
550 measuring suction in unsaturated soils." 1st European Conference on Unsaturated Soils,
551 Durham, UK, July 2-4, 33-52.

552 Ehrgott, J.Q. Jr., Williams, E.M., Windham, J.E., Akers, S.A., Adley, M.D., Graham, S.S., Reed,
553 P.A., & Waddell, T.A. 2010. Tactical Wheeled Vehicle Survivability: Construction and
554 Characterization of Dry Sand Testbeds in Bare Charge Experiments. Technical Report
555 ERDC/GSL-10-15, Vicksburg, MS: U.S. Army Engineer Research and Development Center.

556 Fredlund, D.G., & Rahardjo, H. 1993. Soil Mechanics for Unsaturated Soils. Wiley, NY.

557 Gibson, R.E., & Henkel, D.J. 1954. "Influence of duration of tests at constant rate of strain on
558 measured "drained" strength." Géotechnique, 4(1), 6-15.

559 Hendron, A.J., Davisson, M.T. & Parola, J.F. 1969. Effect of Degree of Saturation on
560 Compressibility of Soils from the Defense Research Establishment Suffield. US Army
561 Engineer Waterways Experiment Station: Vicksburg, MS.

562 Hilf, J.W. 1956. An Investigation of Pore-water Pressure in Compacted Cohesive Soils.
563 Technical Memo No. 654, United States Bureau of Reclamation, Denver, CO.

564 Johnson, G.R., Beissel, S.R., Gerlach, C.A., Stryk, R.A., Holmquist, T.J., Johnson, A.A., Ray,
565 S.E. & Arata, J.J. 2006. User instructions for the 2006 version of the EPIC code. Final report.
566 Network Computing Services Inc. Minneapolis, MN.

567 Jotisankasa, A. 2005. Collapse Behaviour of a Compacted Silty Clay. Ph.D. Thesis, Imperial
568 College London, London, UK.

569 Jotisankasa, A., Ridley, A., Coop, A. (2007). "Collapse behavior of a compacted silty clay in the
570 suction-monitored oedometer apparatus." Journal of Geotechnical and Geoenvironmental
571 Engineering, 133(7), 867-877

572 Jotisankasa, A., Coop, M. & Ridley, A. (2009). "The mechanical behaviour of an unsaturated
573 compacted silty clay." Géotechnique, 59(5), 415-428.

574 Khalili, N., & Lloret, B. 2001. "An elasto plastic model for non-isothermal analysis flow and
575 deformation in unsaturated porous media: foundation." International Journal of Solids and
576 Structures, 38(46-47), 8305-8330.

577 Lee, K.L., & Seed, H.B. 1967. "Drained strength characteristics of sands." Journal of the Soil
578 Mechanics and Foundations Division, 93(SM6), 117-141.

579 Lloret, A., Villar, M.V., Sanchez, M., Gens, A., Pintado, X., & Alonso, E.E. 2003. "Mechanical
580 behaviour of heavily compacted bentonite under high suction changes." Géotechnique, 53(1),
581 27-40.

582 Maatouk, A., Leroueil, S., & La Rochelle. P. 1995. "Yielding and critical state of a collapsible
583 unsaturated silty soil." Géotechnique, 45(3), 465-477.

584 Matyas, E.L., & Radhakrishna, H.S. 1968. "Volume change characteristics of partially saturated
585 soil." Géotechnique, 18(4), 432-448.

586 Mazanti, B.B. & Holland, C.N. 1971. C.N. Study of Soil Behavior under High Pressure:
587 Response of Two Recompacted Soils to Various States of Stress. US Army Engineer
588 Waterways Experiment Station. Contract Report S-70-2.

589 Moral, R.J., Danielson, K.T., & Ehrgott, J.Q. Jr. 2010. Tactical Wheeled Vehicle Survivability:
590 Comparison of Explosive-Soil-Air-Structure Simulations to Experiments using the Impulse
591 Measurement Device. Report ERDC/GSL TR-10-27. US Army Engineer Research and
592 Development Center, Vicksburg, MS.

593 Murphy, D.J. 1971. "High pressure experiments on soil and rock." Proc. Thirteenth U.S.
594 Symposium on Rock Mechanics. E.J. Cording, Ed. New York: ASCE, 1972. 691-715.

595 Schuurman, I.E. 1966. "The compressibility of an air/water mixture and a theoretical relation
596 between the air and water pressure." Géotechnique, 16(4), 269-281.

597 Skempton, A.W. 1961. "Effective stress in soils, concrete, and rocks." International Conference
598 on Pressure and Suction in Soils. Butterworth, London. 4-16.

599 van Genuchten, M.T. 1980. "A closed-form equation for predicting the hydraulic conductivity of
600 unsaturated soils." Soil Science Society of America Journal, 44(5), 892-898.

601 Vesić, A.S., & Clough, G.W. 1968. "Behaviour of granular materials under high stresses."
602 Journal of the Soil Mechanics and Foundations Division. 94(SM3), 313-326.

603 Wang, Z., & Lu, Y. 2003. "Numerical analysis on dynamic deformation mechanism of soils
604 under blast loading." Soil Dynamics and Earthquake Engineering, 23(8), 705-714.

605 Wayllace A., & Lu, N. 2012. "A transient water release and imbibitions method for rapidly
606 measuring wetting and drying soil water retention and hydraulic conductivity functions."
607 Geotechnical Testing Journal. 35(1), 103–117.

608 Wheeler, S.J., & Sivakumar, V. 1992. "A critical state framework for unsaturated soil."
609 Proceedings of the 7th International Conference Expansive Soils (ICES 92), Dallas, TX,
610 August 3-5, 167-172.

611 Zimmerman, H.D., Wagner, M.H., Carney, J.A., & Ito, Y.M. 1987. Effects of Site Geology on
612 Ground Shock Environments: Report 1, Constitutive Models for Materials I2, I3, and W1-
613 W10. Technical Report SL-87-19. Vicksburg, MS: U.S. Army Engineer Waterways
614 Experiment Station.

615 Zimmerman, H.D., Shimano, R.T., & Ito, Y.M. 1992. Early-Time Ground Shock from Buried
616 Conventional Explosives: User's Guide for SABER-PC/CWE. Instruction Report SL-92-1.
617 Vicksburg, MS: U.S. Army Engineer Waterways Experiment Station.

618

619 **LIST OF TABLE AND FIGURE CAPTIONS**

649 Figure 13: Procedures for application of hydro-mechanical stresses for the drained compression
650 tests under constant matric suction
651 Figure 14: Time series of mean effective stress and water outflow from Boulder clay specimens
652 with different initial degrees of saturation during drained compression: (a) S_r = 1.0; (b)
653 S_r = 0.9; (c) S_r = 0.8
654 Figure 15: Volume change versus mean effective stress during drained compression of Boulder
655 clay specimens having different initial degrees of saturation: (a) S_r = 1.0; (b) S_r = 0.9;
656 (c) S_r = 0.8
657 Figure 16: Comparison of the water outflow and total volume change during drained
658 compression of Boulder clay specimens having different initial degrees of saturation
659 Figure 17: Change of degree of saturation during drained compression of unsaturated Boulder
660 clay specimens with different initial degrees of saturation
661 Figure 18: Compression behavior of clay specimens with different initial degrees of saturation:
662 (a) e-logp′ compression curves; (b) e-p′ compression curves under low mean effective
663 stresses; (c) e-p′ compression curves under high mean effective stresses
664 Figure 19: (a) LC curves for different low plasticity soils in terms of total stress; (b) Change of
665 compressibility with the initial degree of saturation
666 Figure 20: (a) Compression curves for Boulder clay specimens having different initial degrees of
667 saturation and different drainage conditions; (b) Change of outflow rate during
668 compression of a saturated Boulder clay specimen
669 Figure 21: Mean effective stress values at pressurized saturation as a function of the initial
670 degree of saturation for different soils
671
672

673 Table 1: Geotechnical properties of Boulder clay

Property	Value
D_{10}	$< 1.7\times10^{-4}$ mm
D_{30}	< 0.001 mm
D_{50}	0.001 mm
Percent fines	100 %
G_s	2.70
Liquid limit, LL	41
Plastic limit, PL	18
Plasticity index, PI	23
Activity, A	0.75
Maximum dry unit weight, γ_{d_max}	17.4 kN/m^3
Optimum water content, w_{opt}	17.5%
Compression index, C_c	0.23
Recompression index, C_r	0.04
Drained friction angle, ϕ'	33˚

674

675 Table 2: Capacity details of the high-pressure syringe pump

Pressure range (MPa)	0.07 ~ 165
Cylinder capacity (ml)	68
Flow rate (ml/min)	0.00001 ~ 25
Flow accuracy	±0.3% of set point
Dimensions (H×W×D, m)	1.03×0.27×0.45

676

677 Table 3: Test variables

Test No.	**Drainage Condition**	**Initial Void Ratio**	**Initial Degree of Saturation, S_r**	**Gravimetric Water Content, w (%)**	**B Value / Initial Suction (kPa)**	**Initial Volumes of Soil Phases (mm^3)** V_s	V_v	V_a
1-1	Undrained	0.51	1.00	18.9*	0.97 / -	189,566	96,420	7,489
1-2	Undrained	0.51	0.92	17.2	- / 80	189,645	96,044	7,324
1-3	Undrained	0.51	0.84	15.7	- / 89	188,899	95,608	15,435
2-1	Drained	0.51	1.00	18.9*	0.95 / -	189,879	96,107	8,021
2-2	Drained	0.51	0.92	17.3	- / 80	189,156	95,699	7,399
2-3	Drained	0.51	0.82	15.5	- / 89	188,704	97,004	17,815

678 *Compacted at w = 17.3% then saturated using upward flow under vacuum to w = 18.9%

679 Table 4: Summary of test results

Test No.		**1-1**	**1-2**	**1-3**	**2-1**	**2-2**	**2-3**
Drainage condition		Undrained	Undrained	Undrained	Drained	Drained	Drained
Water content (%) (Initial/Final)		17.4 / 18.1	17.3 / 16.8	15.7 / 14.6	17.2 / 11.2	17.3 / 9.91	15.5 / 9.21
Degree of saturation, S_r (Initial/Final)		0.92 / 1.00	0.92 / 0.98	0.84 / 0.81	1.00 / 0.96	0.92 / 1.00	0.82 / 1.00
λ_s (C_c/ln10)		-	-	-	0.0279	0.0611	0.0737
κ (k_u) (C_s/ln10)		0.0044	0.0067	0.0131	0.0053	0.0060	0.0059
Mean effective preconsolidation stress, p'_c (kPa)		19,000	1,100	250	110	380	580
Volume of soil phase (mm^3) (Initial/Final)	**V_s**	189,566 / 191,759	189,645 / 187,044	188,259 / 187,278	189,879 / 188,067	189,156 / 187,422	188,704 / 187,707
	V_v	96,420 / 93,835	96,044 / 86,346	96,248 / 87,460	96,107 / 59,367	95,699 / 50,160	95,505 / 46,739
	V_a	7489 / -	7,324 / 1,576	16,347 / 13,780	8,021 / 2,667	7,398 / -	16,315 / -
Void ratio (Initial / Final)		0.51 / 0.49	0.51 / 0.46	0.51 / 0.47	0.51 / 0.32	0.51 / 0.21	0.51 / 0.25
Mean effective stress at pressurized saturation, p'_{ps} (kPa)		-	6,000	9,000	-	1,100	1,800

680

681 Table 5: Comparison between fitting parameters for the LC yield curve function of Alonso et al.

682 (1990) for different low plasticity clays

Parameters	Boulder clay (this study)	Silty clay (Jotisankasa et al. 2009)
r	300	60
β	0.08 MPa^{-1}	0.05 MPa^{-1}
p^c	2 MPa	3.50 MPa
p_0^*	0.11 MPa	0.04 MPa

683

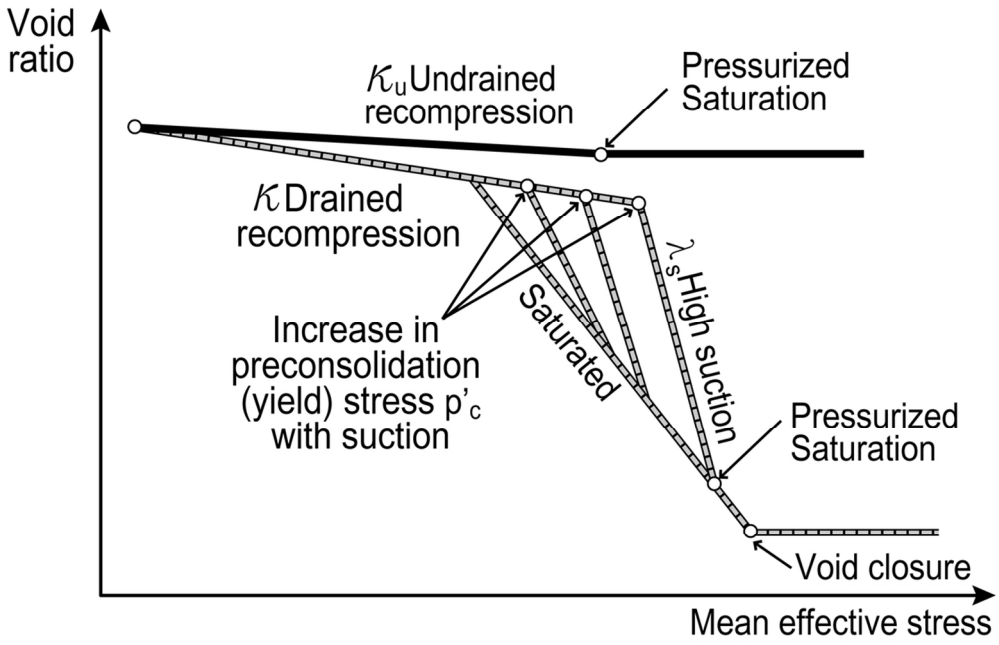

56x35mm (600 x 600 DPI)

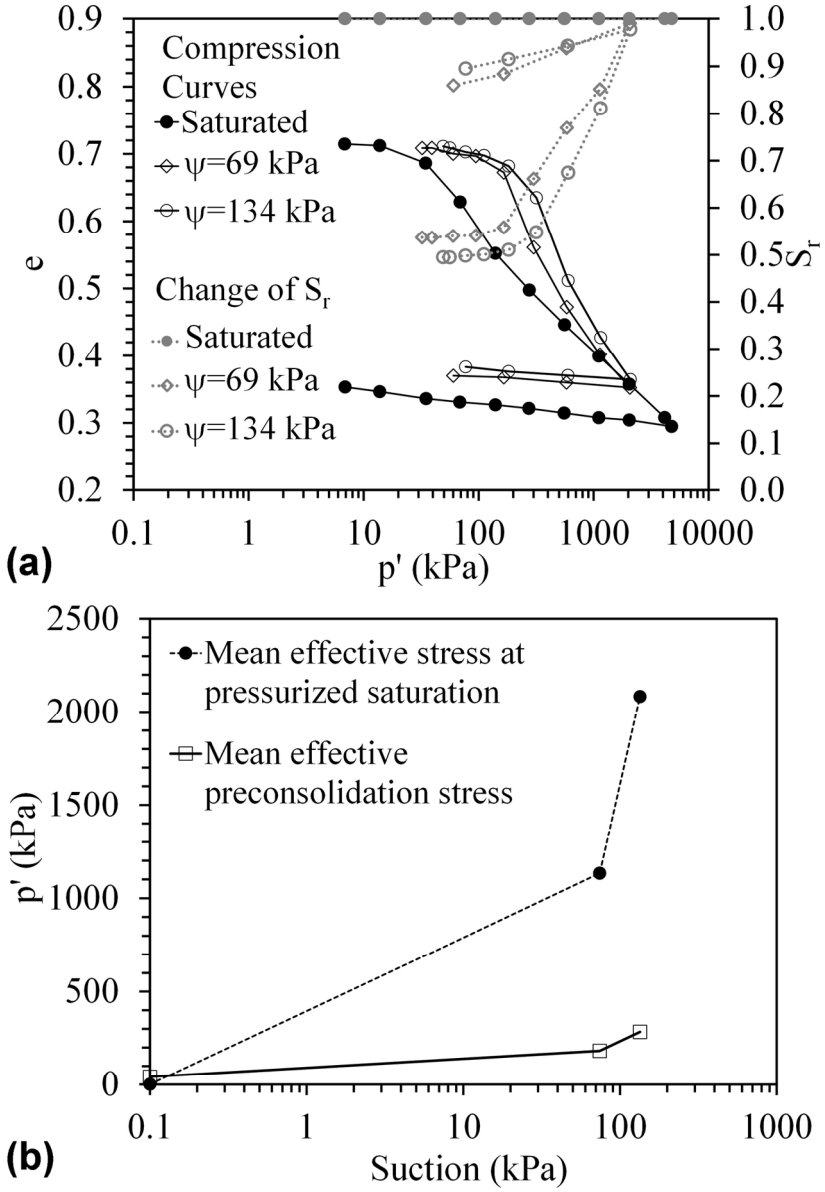

129x189mm (300 x 300 DPI)

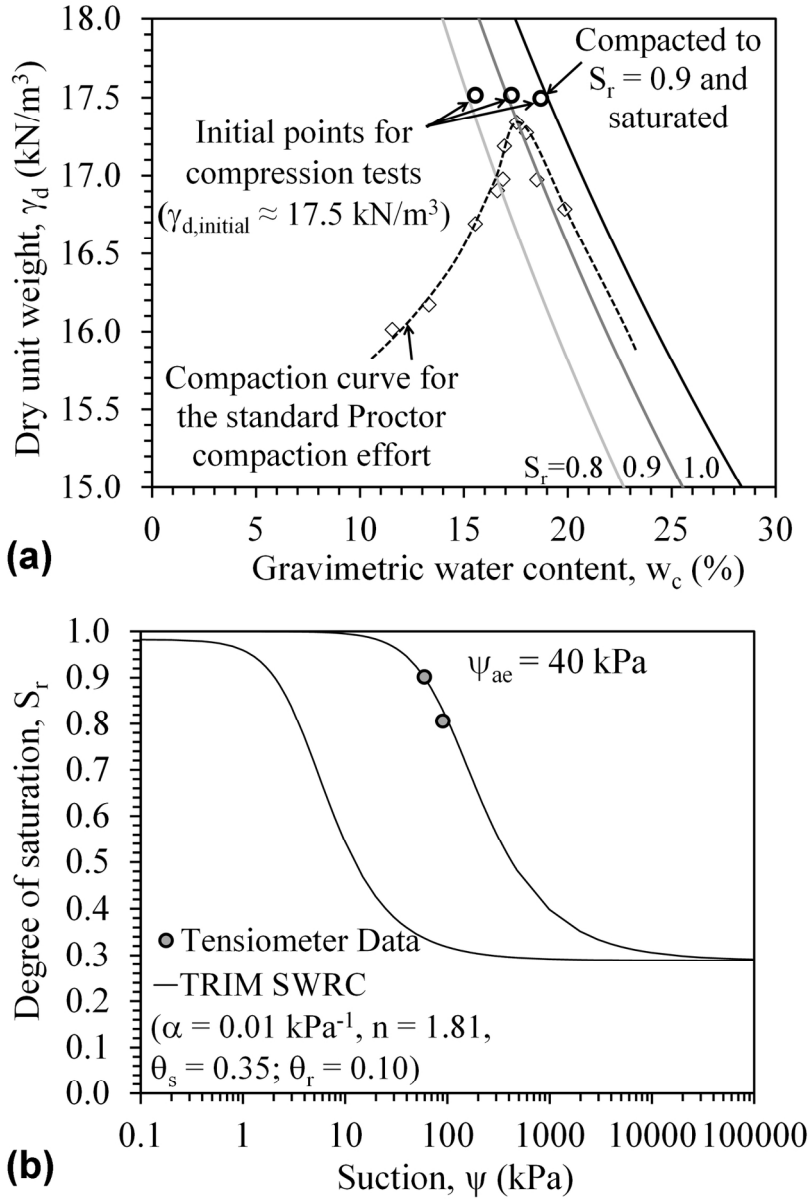

131x193mm (300 x 300 DPI)

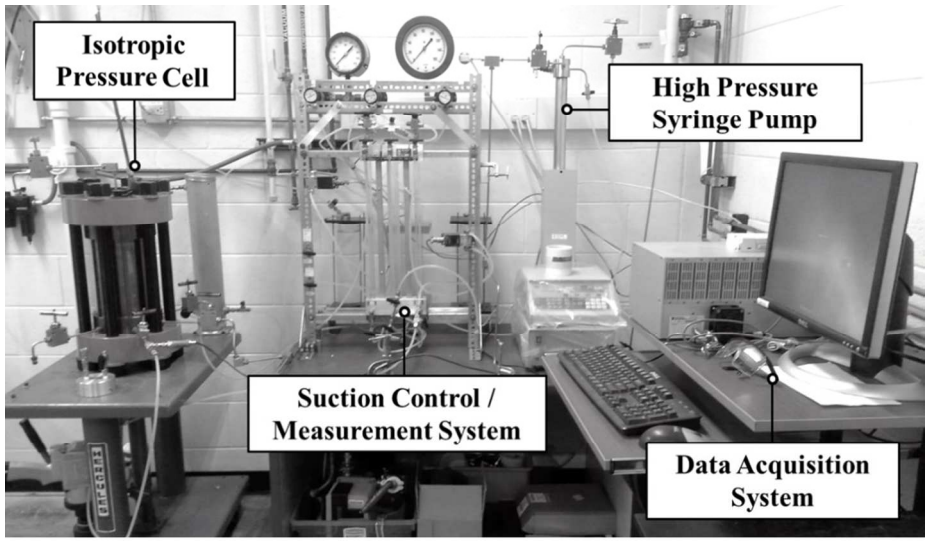

(a)

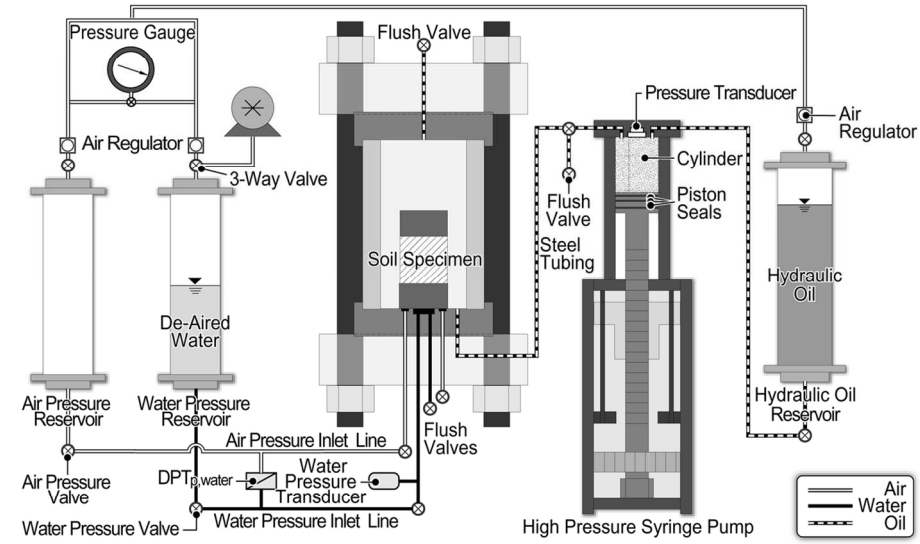

(b)

116x151mm (300 x 300 DPI)

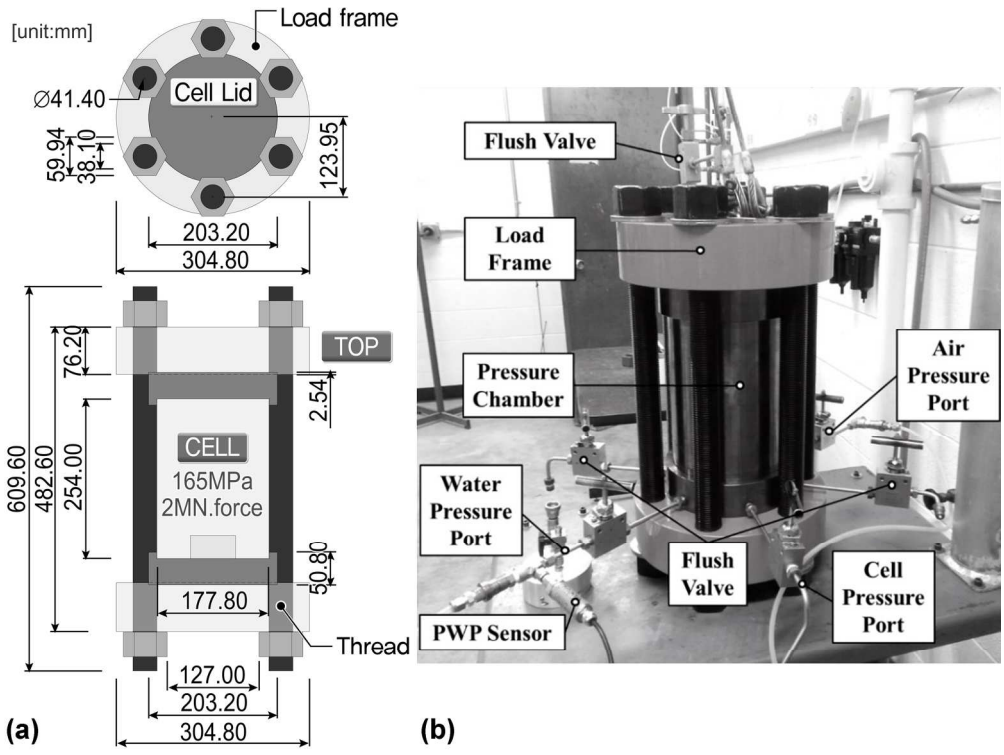

95x71mm (600 x 600 DPI)

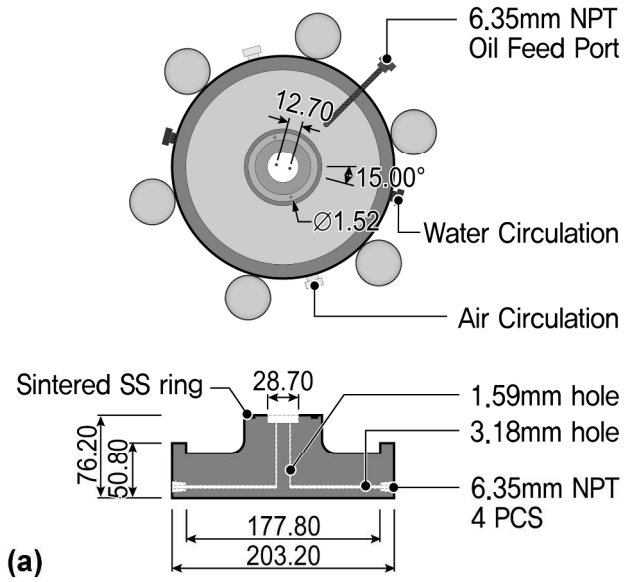

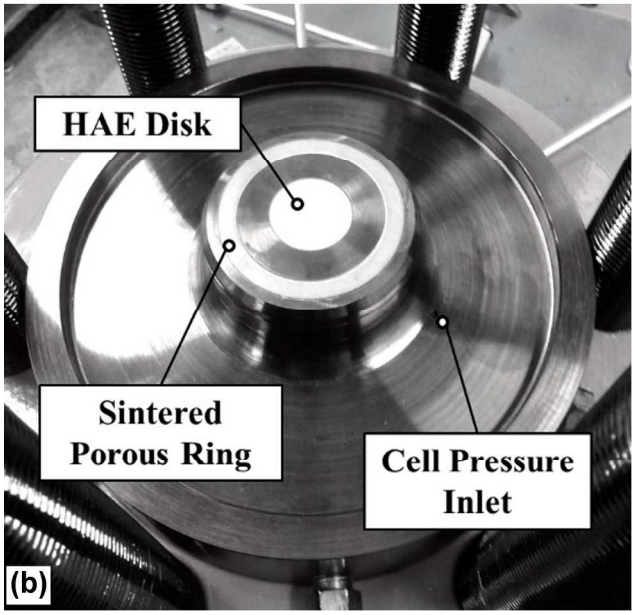

170x325mm (300 x 300 DPI)

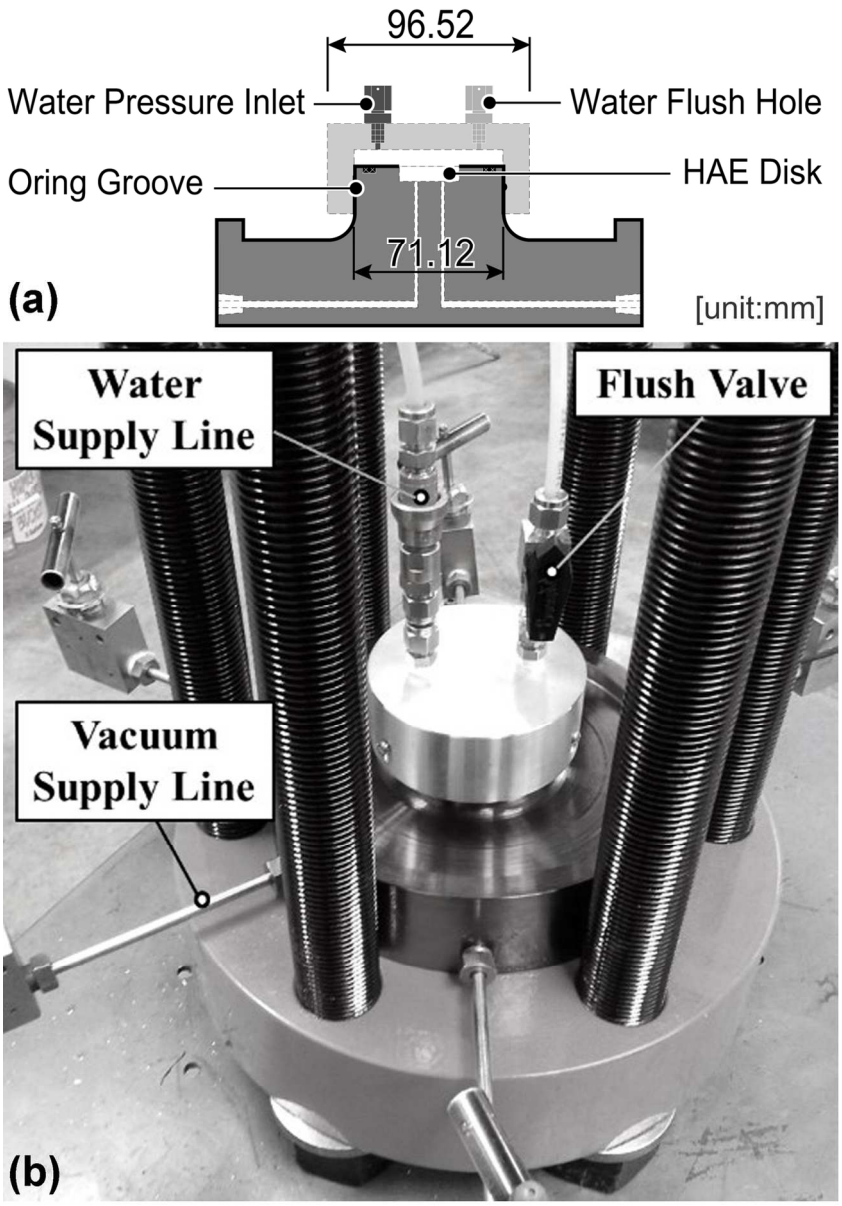

120x172mm (300 x 300 DPI)

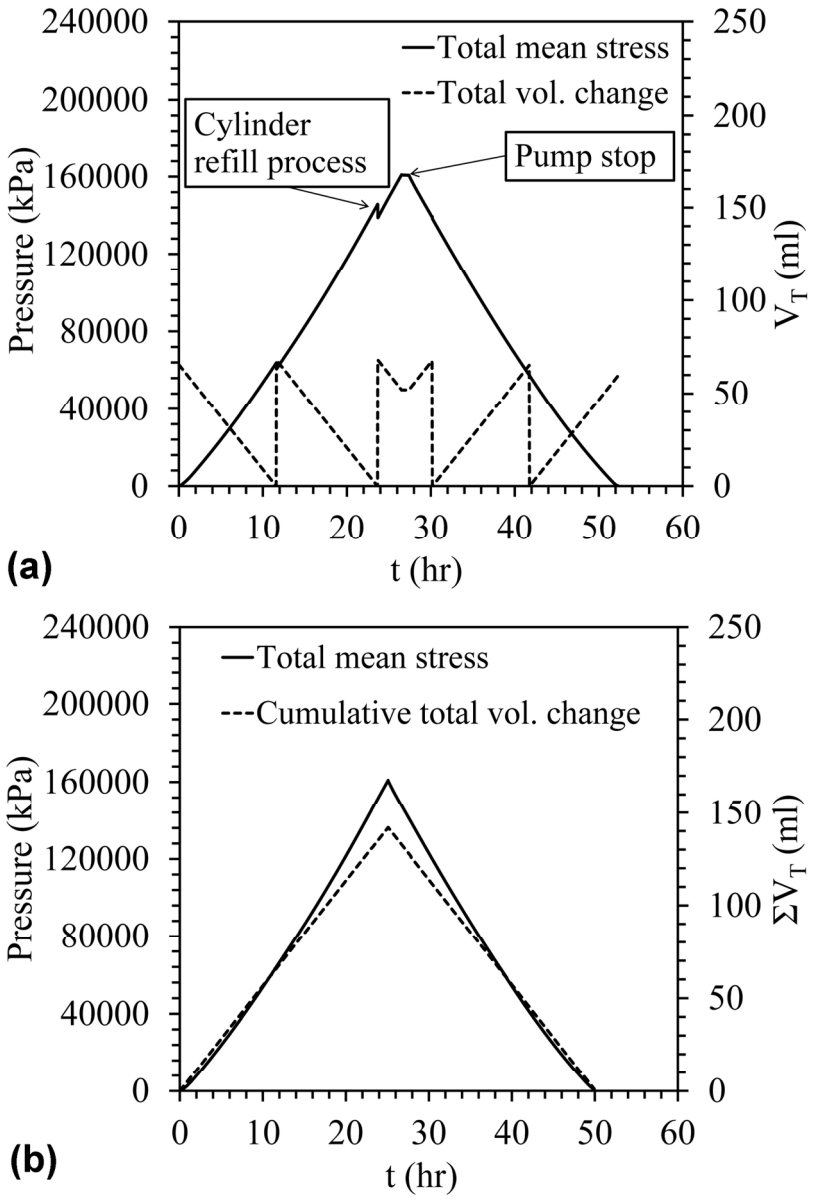

132x198mm (300 x 300 DPI)

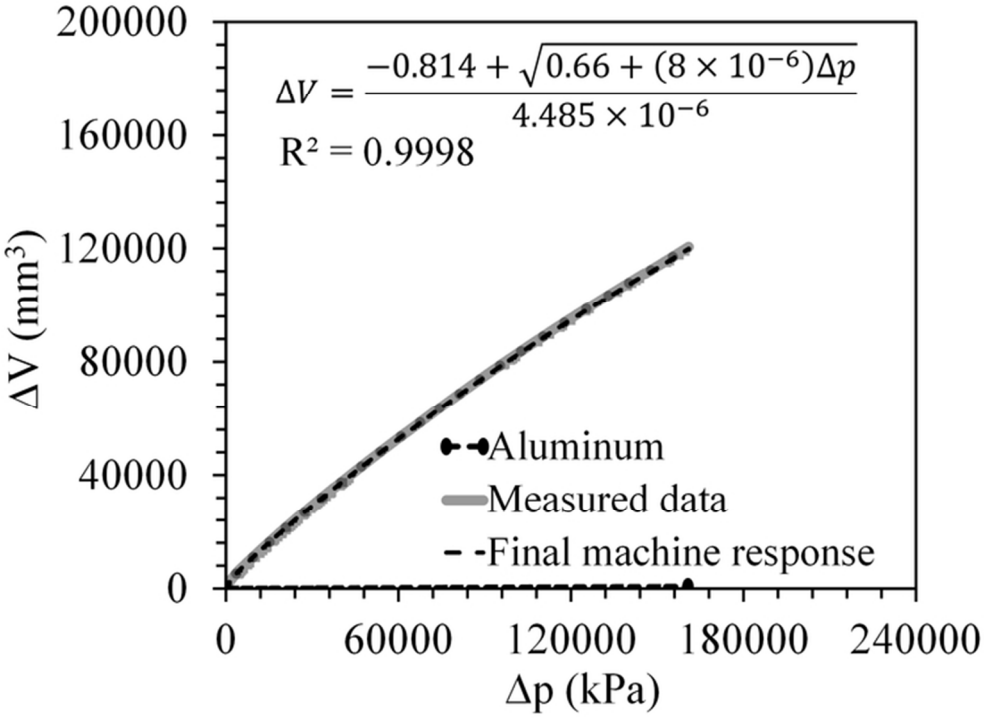

64x47mm (300 x 300 DPI)

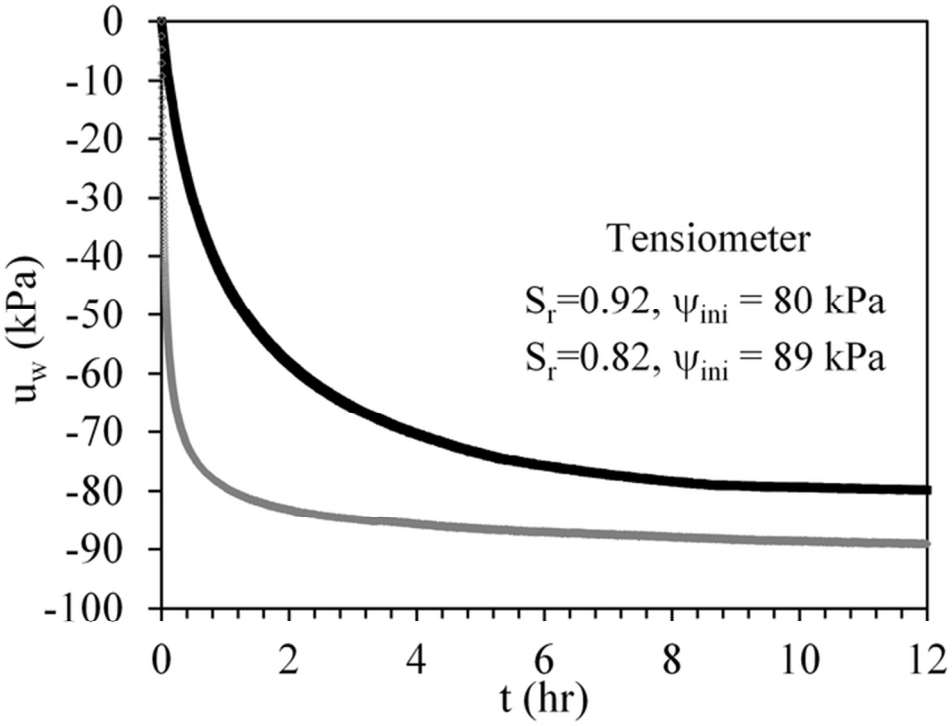

64x47mm (300 x 300 DPI)

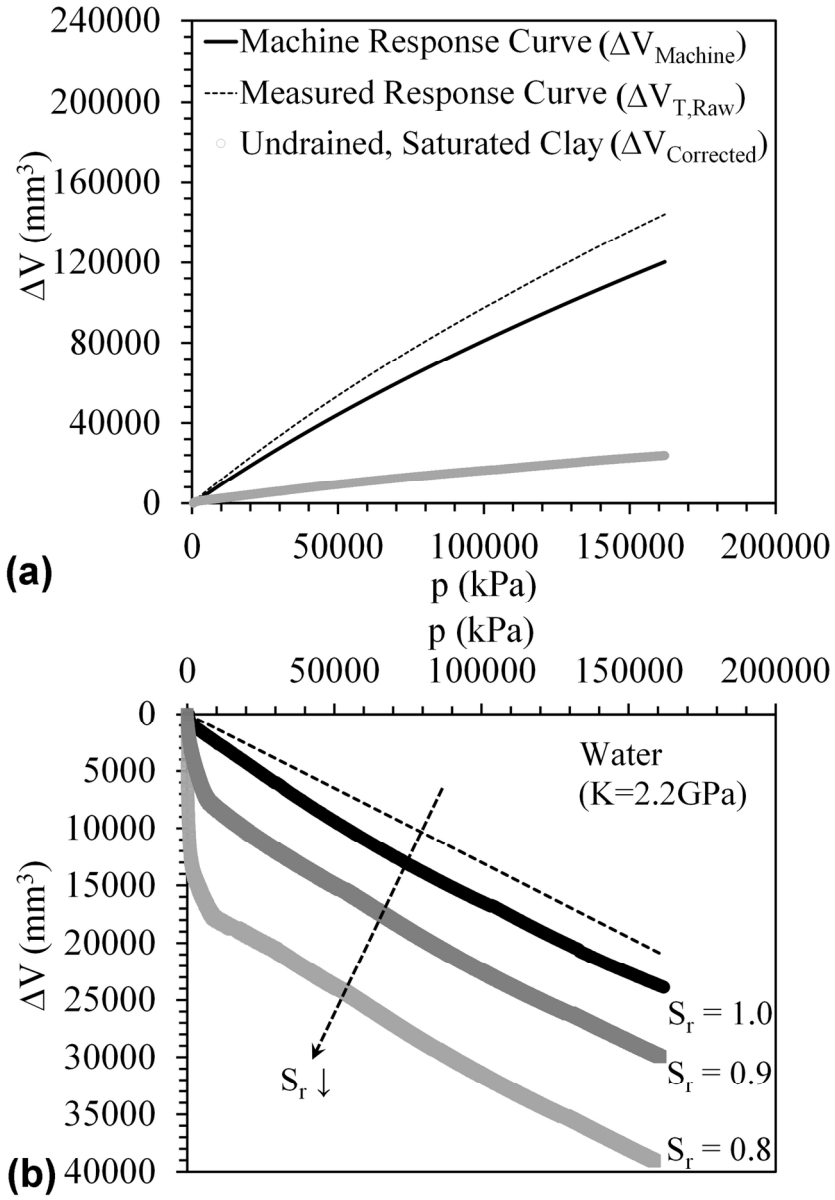

128x184mm (300 x 300 DPI)

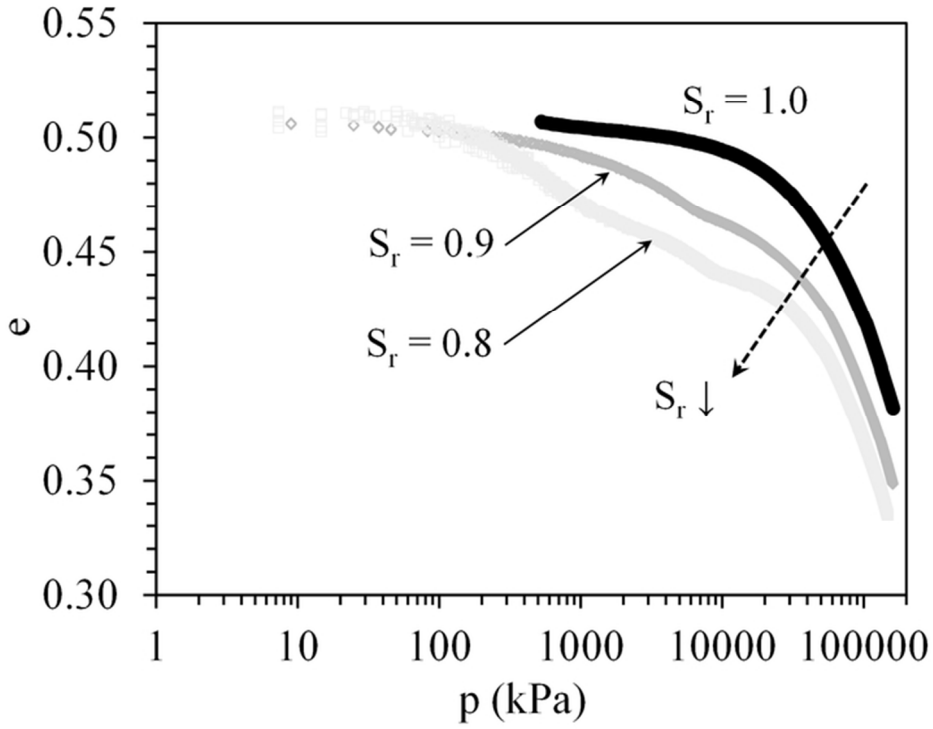

65x47mm (300 x 300 DPI)

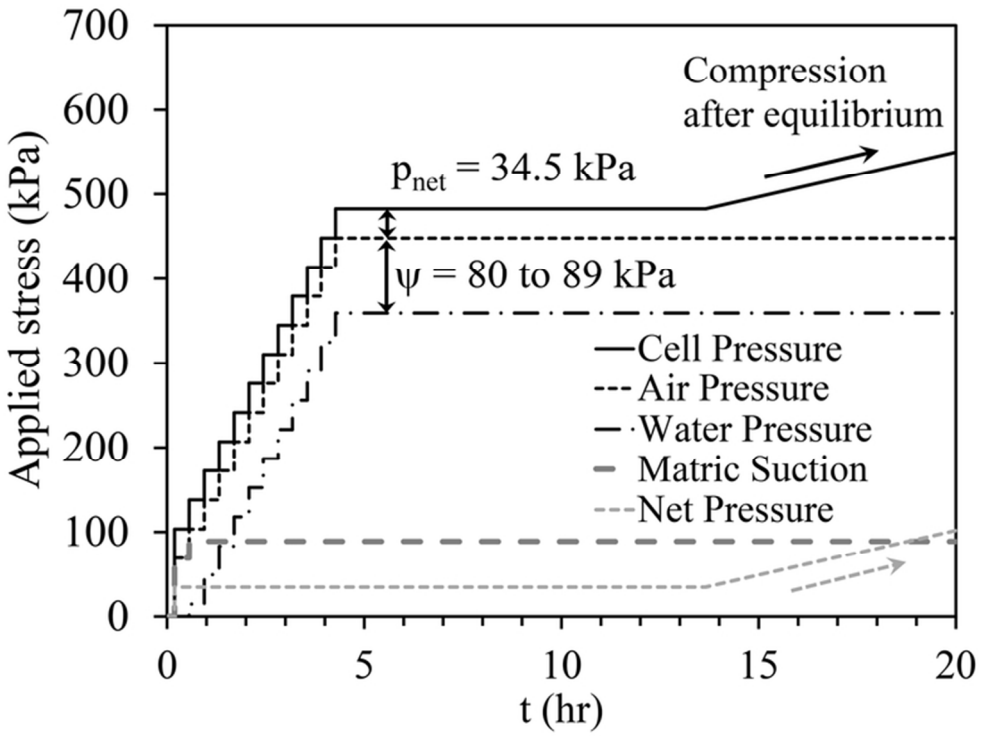

67x51mm (300 x 300 DPI)

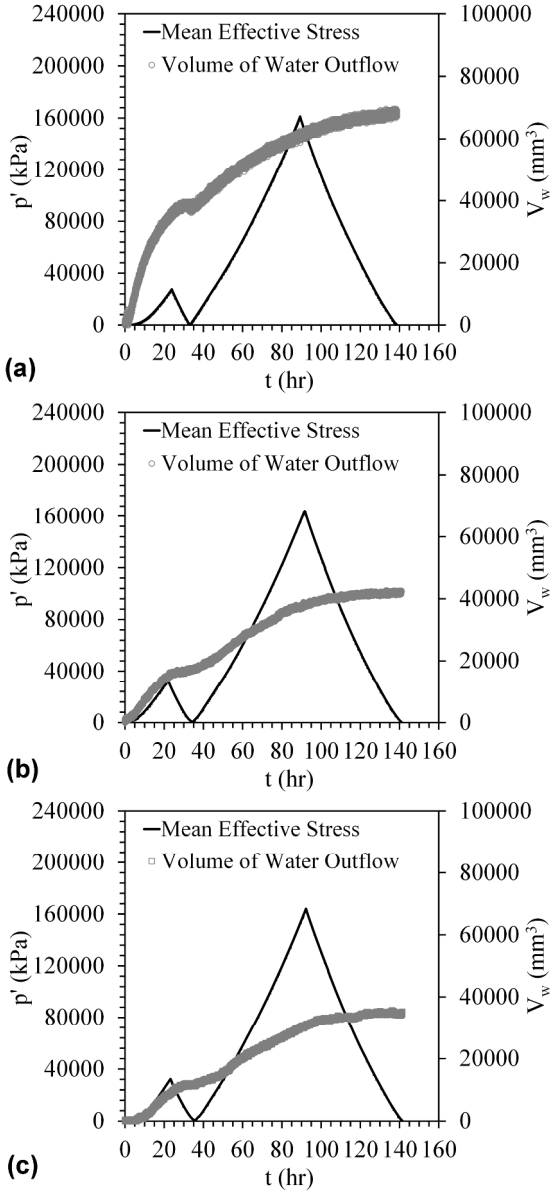

194x426mm (300 x 300 DPI)

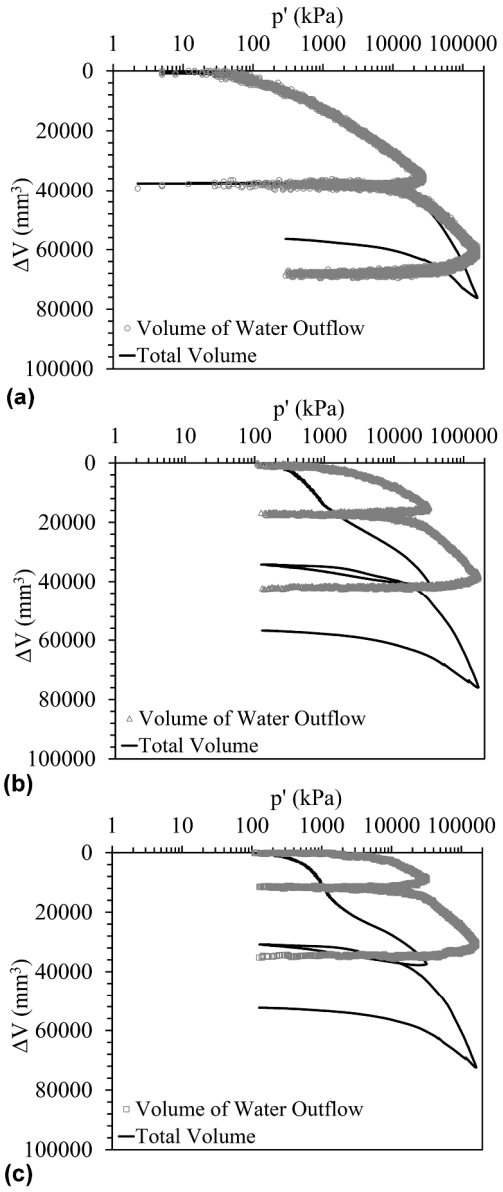

212x508mm (300 x 300 DPI)

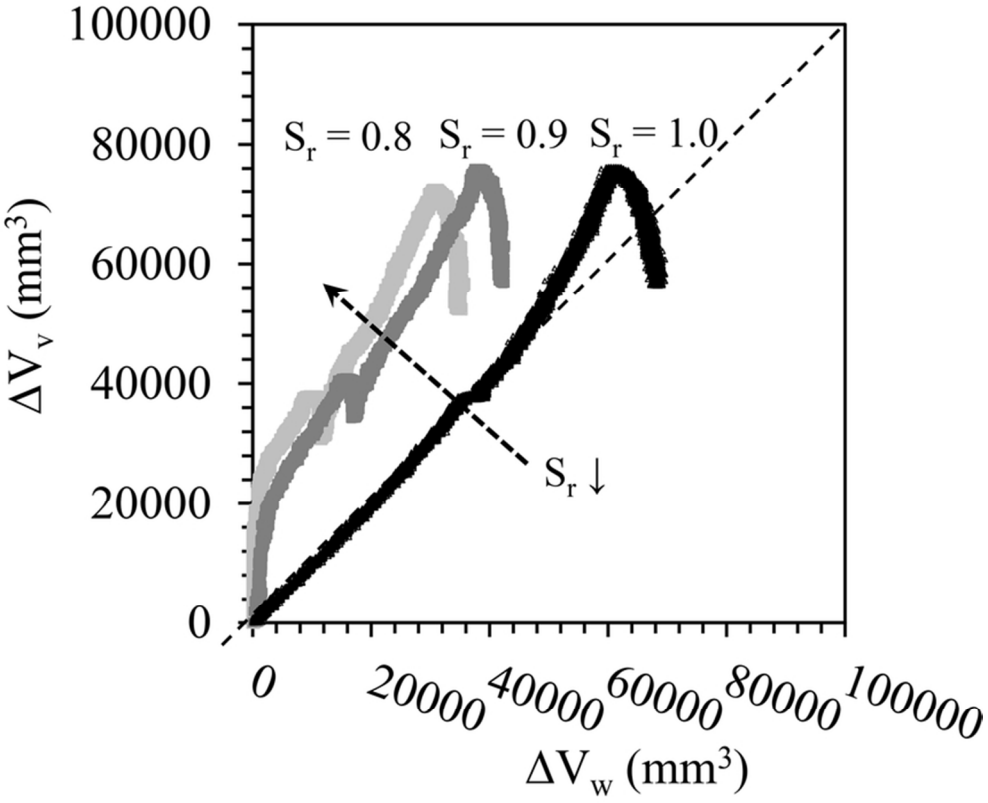

73x61mm (300 x 300 DPI)

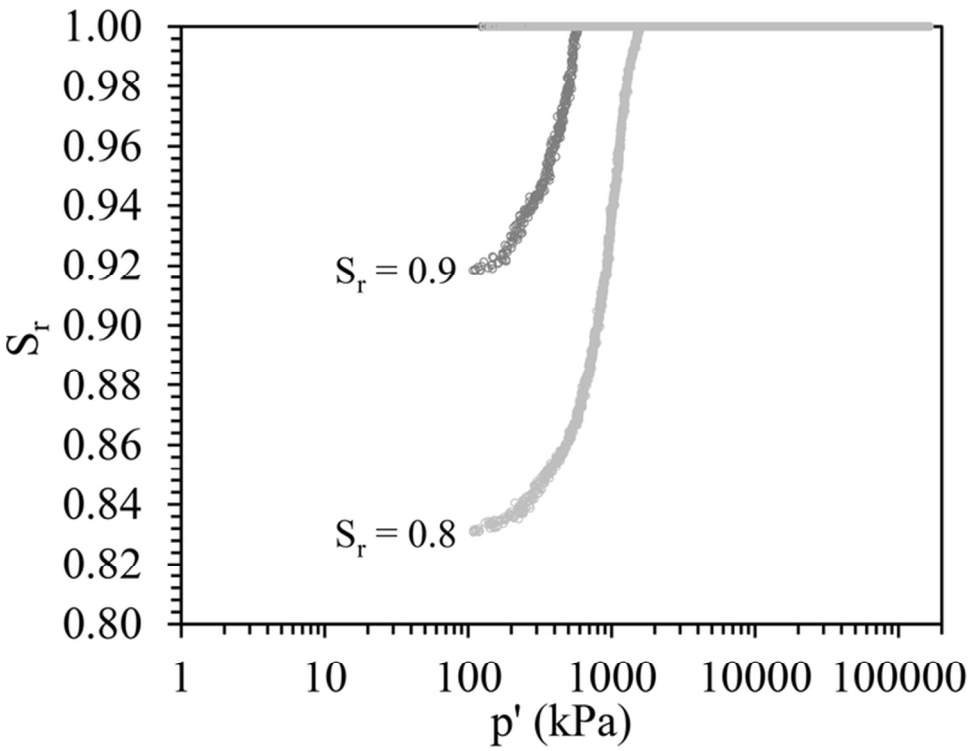

68x53mm (300 x 300 DPI)

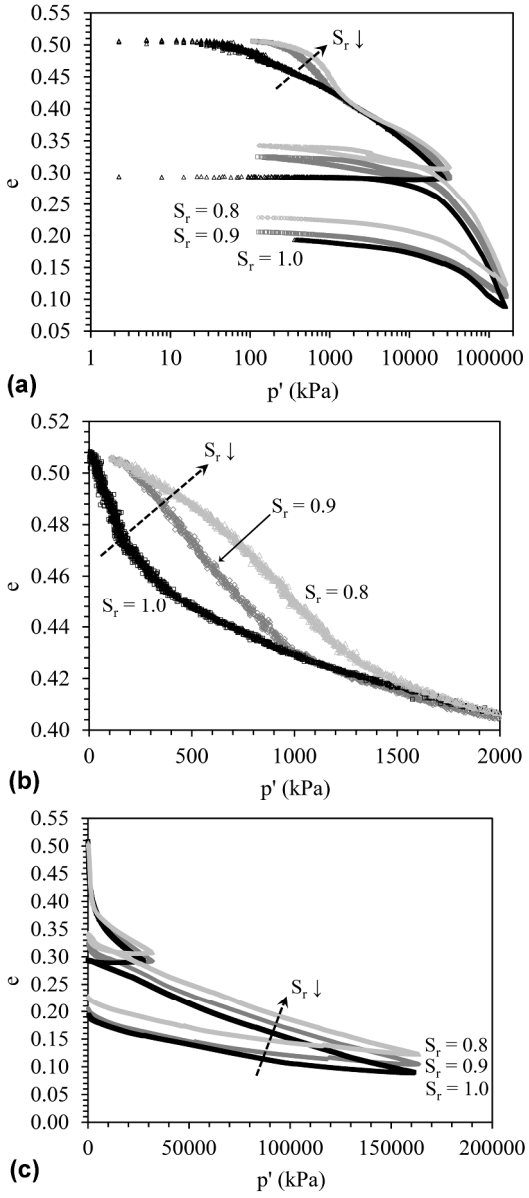

203x464mm (300 x 300 DPI)

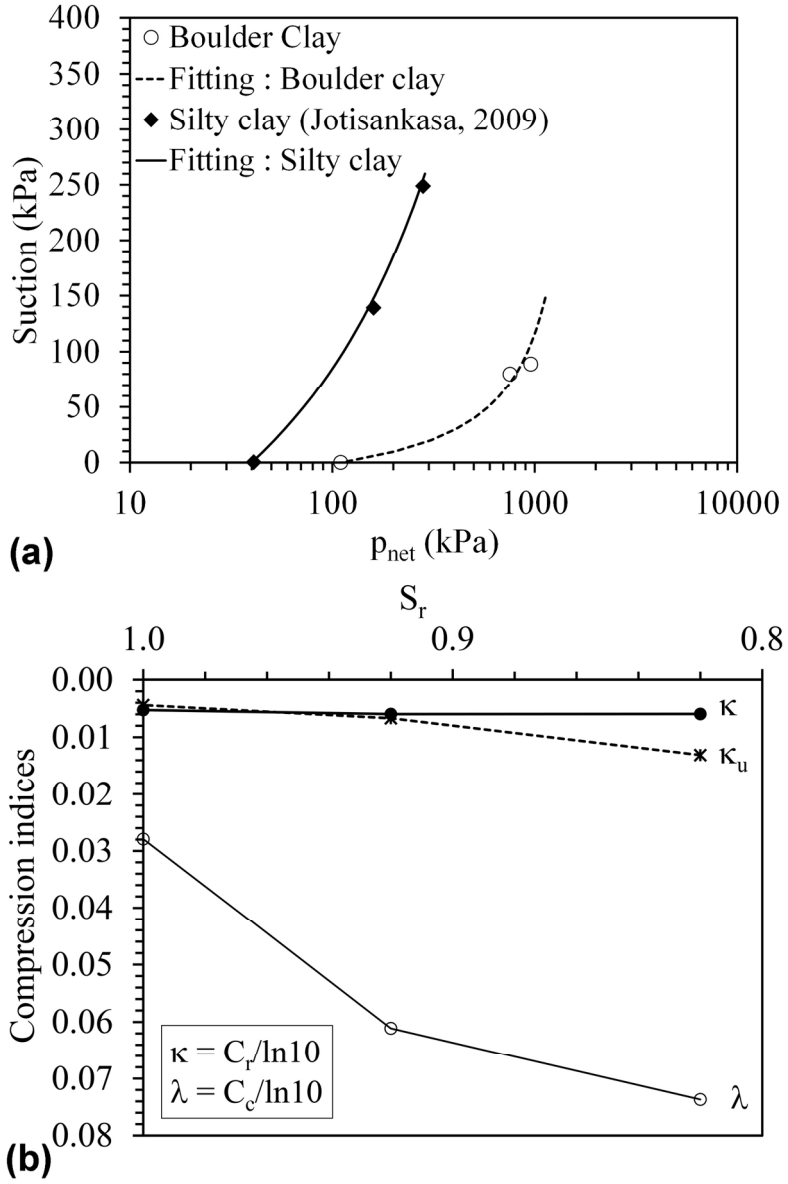

135x207mm (300 x 300 DPI)

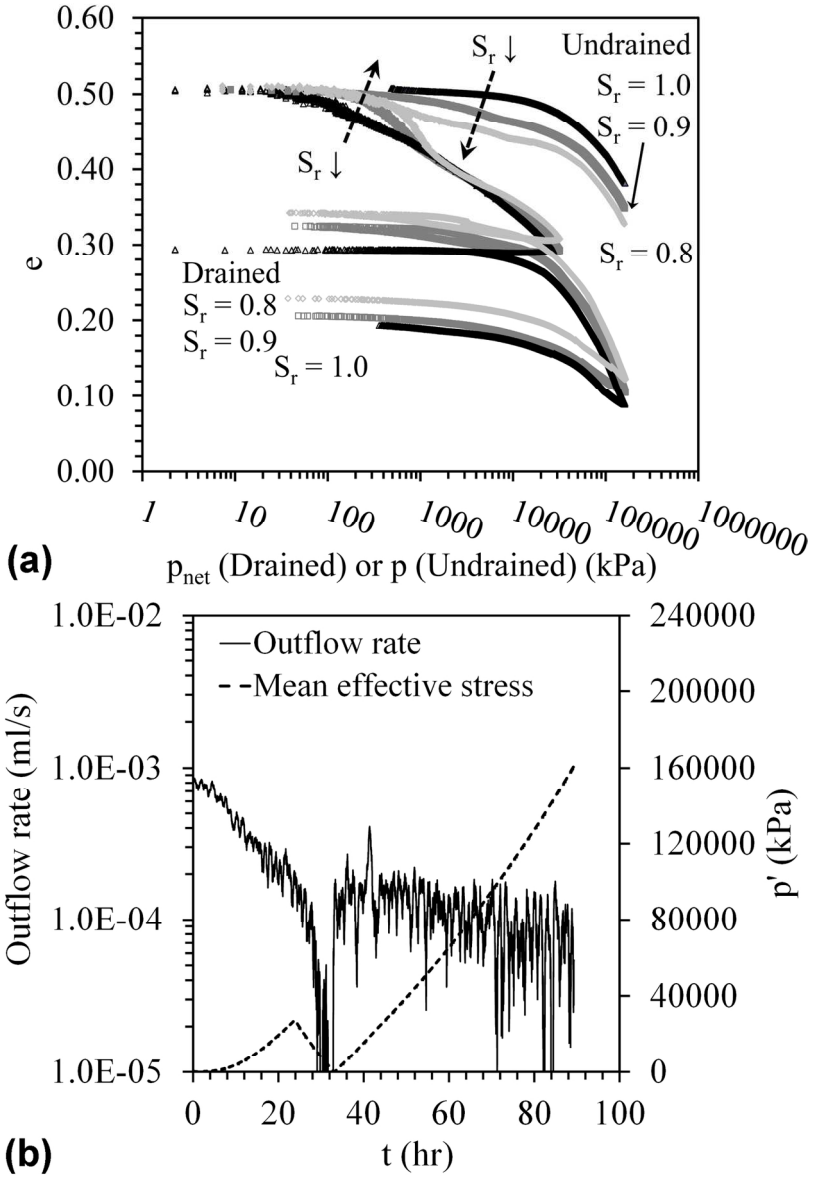

132x197mm (300 x 300 DPI)

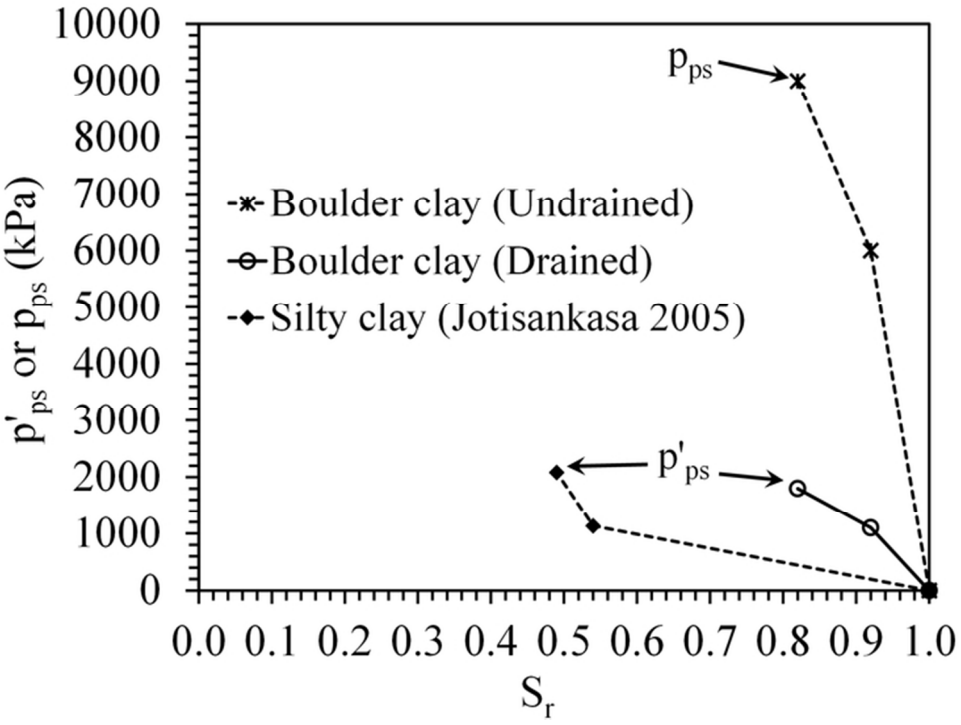

64x46mm (300 x 300 DPI)